J Sol-Gel Sci Technol (2008) 46:166–175
DOI 10.1007/s10971-008-1718-z

ORIGINAL PAPER

Synthesis, structure and bioactivity of pHEMA/SiO_2 hybrids derived through in situ sol–gel process

G. Luciani · A. Costantini · B. Silvestri · F. Tescione · F. Branda · A. Pezzella

Received: 17 October 2007 / Accepted: 25 February 2008 / Published online: 18 March 2008

Abstract A novel procedure to synthesize poly(2-Hydroxyethylmethacrylate)-silica blend hybrids is presented. Methacrylate monomers bearing an alkoxysilyl unit, prepared by Michael addition of 2-Hydroxyethylmethacrylate (HEMA) to 3-Aminopropyltriethoxysilane (APTS), were employed. By ^{13}C NMR and mass analysis it was possible to establish the formation of coupling hybrid species. A hybrid material, with final concentration of 30% w/w of silica gel to the mass of polymer, was obtained through basic catalysed sol–gel process of tetraethoxysilane (TEOS) and the alkoxysilyl unit of the hybrid monomer, followed by in situ free-radical polymerization. Optical transparency and higher glass transition temperature than pHEMA suggest an increase in either density or strong interphase interactions. Moreover, pHEMA/SiO_2 gel blend hybrid exhibits better thermal stability than the as-prepared polymer. Morphology and structure were studied through scanning electron microscopy (SEM), transmission electron spectroscopy (TEM), and dynamic light scattering (DLS). The structure of the hybrid consisted of nanosilica, 10 nm in mean diameter, uniformly dispersed in the pHEMA phase with strong interactions between the phases. Nevertheless, the swelling ratio of the hybrid was comparable to pHEMA. Using FT-IR spectroscopy, SEM and energy dispersive system (EDS), XRD analysis in vitro bioactivity of the hybrid, due to the inorganic phase, was ascertained therefore, the obtained hybrid can be used to make bioactive scaffold for bone engineering.

Keywords Bioactive materials · Hydrogels · pHEMA/silica blend hybrids · SiO_2 nanoparticles · Michael addition

G. Luciani (✉) · A. Costantini · F. Tescione · F. Branda
Dipartimento di Ingegneria dei Materiali e della Produzione, Università di Napoli Federico II, Piazzale Tecchio, 80, Naples 80125, Italy
e-mail: luciani@unina.it

B. Silvestri
Interdisciplinary Centre of Biomedical Materials (CRIB), Università of Napoli Federico II, Piazzale Tecchio, 80, Naples 80125, Italy

A. Pezzella
Dipartimento di Chimica Organica e Biochimica, Università di Napoli Federico II, Complesso Universitario Monte S.Angelo via Cinthia 4, Naples 80126, Italy

1 Introduction

The sol–gel process, with its associated mild conditions, offers a new synthetic route to produce organic–inorganic composite materials, by mixing metal alkoxides with monomers to be polymerized or polymers [1–3]. Since the mid-1980s, when the first sol–gel hybrids where obtained by mixing linear polymer chains with silica precursors [4–6] a great many composites have been produced for a variety of applications such as optical devices [7–9], organically modified ceramic materials [10–12], reinforced elastomers and plastics [13], bioactive materials [14–16], chemical/biomedical sensors [17, 18] and many others.

Poly-(2-Hydroxyethylmethacrylate) (pHEMA), a biocompatible hydrogel proposed as early as 1960 [19–21] is yet today an outstanding material for biomedical application. It is used to make ophthalmic prostheses (contact or intraocular lenses), vascular prostheses, drug delivery and soft-tissue replacement [22].

p-HEMA, as an hydrogel, can imbibe large amounts of water by swelling without dissolving, thus letting: tissue in-growth; high permeability to small molecules to have highly purified networks; soft consistency, which

minimizes mechanical frictional irritation to surrounding tissues; low interfacial tension between the hydrogel and the aqueous solution that can reduce proteins absorption to the gel; and a large number of morphologies.

Three types of attachment to living tissues are possible: biological fixation, which is due to bone or tissue in growth; morphological fixation, linked to the forces that are generated on the swelling when the hydrogel is placed in a constrained space; bioactive fixation, that has the biomaterial bound to the living tissue, through an apatite layer [23, 24].

Bioactive fixation can be obtained by surface modification of pHEMA, this was performed in the past through the biomimetic method [25, 26].

Bioactive pHEMA-silica hybrids can be produced either by addition of silica nanoparticles to HEMA monomer/pHEMA solution [14, 27] or using pHEMA solutions and inorganic precursors such as tetraethoxysilane (TEOS) through in situ sol–gel processes [16], or by polymerization of organic–inorganic monomers [28]. Hybrid organic–inorganic monomers are materials that can be polymerized both at their "organic" functionality as well as at the "inorganic" reactive group, usually an alkoxysilyl moiety. Such compounds offer the possibility of simultaneous or successive radical polymerization and alkoxysilane condensation due to their orthogonal cross-linking chemistry.

In the present study we report the synthesis of a hybrid monomer of HEMA and 3-Aminopropyltriethoxysilane (APTS), as well as its use to synthesize hybrid *blend* materials through basic catalysed hydrolysis and condensation of its inorganic reactive group and TEOS, followed by in situ radical–radical polymerization of 2-Hydroxyethylmethacrylate (HEMA).

The occurrence of a coupling reaction between HEMA and APTS to give the hybrid monomer is proved by NMR, mass and FT-IR analysis.

The hybrid *blend* material has been characterized as far as concerns composition by thermogravimetric analysis (TG) and FT-IR, swelling behaviour, glass transition temperature using differential thermal analysis (DTA), morphology and structure through scanning electron microscopy (SEM) and transmission electron microscopy (TEM). Silica particles size has been measured through dynamic light scattering (DLS) analysis. Moreover, in vitro bioactivity of the hybrid material has been studied, using FT-IR spectroscopy, XRD analysis, SEM and energy dispersive system (EDS).

2 Materials and methods

2.1 Materials

2-Hydroxyethylmethacrylate (HEMA), the initiator α-α′azoisobutyronitrile (AIBN) and ethanol were supplied by Fluka (Milan, Italy). TEOS, 3-Aminopropyltriethoxysylane (APTS), ammonia solution in ethyl alcohol, $NaHCO_3$, KCl, $K_2HPO_4 \cdot 3H_2O$, $MgCl_2 \cdot 6H_2O$, $CaCl_2$ and Na_2SO_4 were purchased by Sigma–Aldrich (Milan, Italy).

2.2 Synthesis and characterization of hybrid monomers

A mixture of 0.812 mL of HEMA and 1.57 mL of APTS was prepared. HEMA and APTS amounts were chosen so as to have equal moles of both reagents.

The solvent free reaction of HEMA and APTS was carried out in thermostat oven and the progress followed by spectral analysis of the crude mixture (IE-MS; ^{1}H- and ^{13}C-NMR) after sample withdrawal at different times. For a faster ^{13}C spectra achievement proton decoupled spectra were acquired with consequent differences in signal intensities as function of proton substitution: substituted carbons sowing weak signals while $-CH_3$ and $=CH_2$ groups featuring higher signal intensity. Indeed focusing on diagnostic signals allowed to get an adequate quantitative determination for the scope of this monitoring.

ESI+/MS and ESI−/MS spectra were obtained in 2% formic acid–methanol 1:1 v/v and water–methanol 1:1 v/v, respectively. ^{1}H and ^{13}C NMR spectra were obtained at 400 and 100 MHz, respectively on Bruker DPX-400, using standard pulse program sequences (proton decoupled pulse programs were employed for the acquisition of all ^{13}C spectra).

The mixture used to prepare hybrid material, was kept at 40 °C in a thermostatic bath for 6 days and then cooled to room temperature.

2.3 Synthesis of hybrid material

The procedure used for the preparation of the hybrid with a concentration of 30% of silica to the mass of the polymer, can be described as follows. First, 1.50 mL of TEOS and 1.69 mL of HEMA monomer were dissolved in the mixture of the hybrid monomer (solution 1). Then 3.94 mL of NH_3 solution in ethanol, 2.0 M and 2.84 mL of water were added to solution 1 (solution 2). The mixture was stirred at room temperature for 30 min, then 2.7 mg of the free-radical initiator (AIBN) were added so as to have a concentration of 0.1% w/w based on the weight of HEMA monomer. The mixture was stirred for 20 min at room temperature. Then, it was opened and poured into a thermostatic bath at 60 °C for 2 h to remove ammonia and most water and ethanol. Finally, it was sealed and cured at 80 °C overnight and at 90 °C for 2 h, in a forced-air circulating oven. After curing, the resulting hybrids were washed with distilled water for 3 weeks, to remove residual monomers and then dried in a forced air circulation oven at 70 °C for 24 h. All samples appeared transparent and quite rigid.

2.4 Materials characterization

SEM images of samples were obtained on Leica Stereoscan 440 microscope, equipped with an energy dispersive analytical system (EDS) INCA Energy 200—Oxford Instruments. As prepared samples were fractured and fractured surfaces were gold-coated before observation. Samples soaked in SBF, were carbon-coated before SEM observation.

Fourier transform infrared (FTIR) transmittance spectra were recorded in the 400–4,000 cm^{-1} using a Nexus FT-IR spectrometer using either a single reflection attenuated total reflectance (ATR) accessory or an in situ diffuse reflectance (DRIFT) system with a resolution of 4 cm^{-1} and 20 scans.

Samples composition was determined by thermal decomposition in a thermogravimetric apparatus, Netzsch TG209, at a heating rate of 10 °C/min under a nitrogen atmosphere.

Differential scanning calorimetry (DSC) was performed on a Netzsch 404 M heat flux apparatus under N_2 flow from room temperature to 250 °C at a heating rate of 10 °C/min.

The polymerized silica particles size and distribution were measured by DLS analysis method. Two hours later mixing, a 1.5 mL solution before the addition of AIBN, was injected into the quartz cuvette and illuminated by a water-cooled spectra-physics argon laser operating at 488 nm. The system was equipped with Glan Thompson polarizer and a gradient index lens optical fiber. The detection system was placed at 90° scattering angle. The signal was analysed by a ALV/SO-SIPD detector using two photomultipliers and a beamsplitter cube for setting a PSEUDO CROSS correlation detection in order to increase the accuracy in the detection of very fast processes. The correlator is an ALV-6010/200 multiple tau digital correlator with a minimum realtime sampling time of 5 ns.

Samples for TEM were sectioned with a diamond knife at 23 °C. TEM was performed using a PHILIPS EM208S microscope, equipped with a MegaView camera for digital acquisition of images.

X-ray diffraction (XRD) experiments were performed in a Philips PW 1830 instrument, with a goniometer Philips PW 3020 and a control unit Philips PW 3710, Cu Kα radiation.

2.5 In vitro studies in SBF

An SBF with ion composition nearly equal to blood plasma (Table 1) was prepared by dissolving reagent grade NaCl, $NaHCO_3$, KCl, $K_2HPO_4 \cdot 3H_2O$, $MgCl_2 \cdot 6H_2O$, $CaCl_2$ and Na_2SO_4 in distilled water as reported by other researchers [29, 30]. It was buffered at pH 7.25 by using trishydroxymethyl-aminomethane (Trizma base) and trishydroxymethyl-aminomethane hydrochloric acid (Trizma–HCl).

Table 1 Ion concentration (mM) of simulated body fluid (SBF) and blood plasma

Ion	Simulated body fluid	Blood plasma
Na^+	142.0	142.0
K^+	5.0	5.0
Mg^{2+}	1.5	1.5
Ca^{2+}	2.5	2.5
Cl^-	147.8	103.0
HCO_3^-	4.2	27.0
HPO_4^{2-}	1.0	1.0
SO_4^{2-}	0.5	0.5

In vitro tests were carried out on bulk samples, at 37 °C. The ratio of exposed surface area to solution volume was kept at 50 mm^2 mL^{-1}. The specimens were soaked for various times and solution was exchanged every 2 days. They were then removed from solution, washed with distilled water and dried at room temperature.

3 Results

Figure 1 shows ^{13}C NMR spectra of pure HEMA, APTS (Fig. 1), and their mixture at different reaction times (Fig. 1). ^{13}C NMR chemical shifts and functional group assignment of HEMA and APTS in $CDCl_3$ are reported in Table 2.

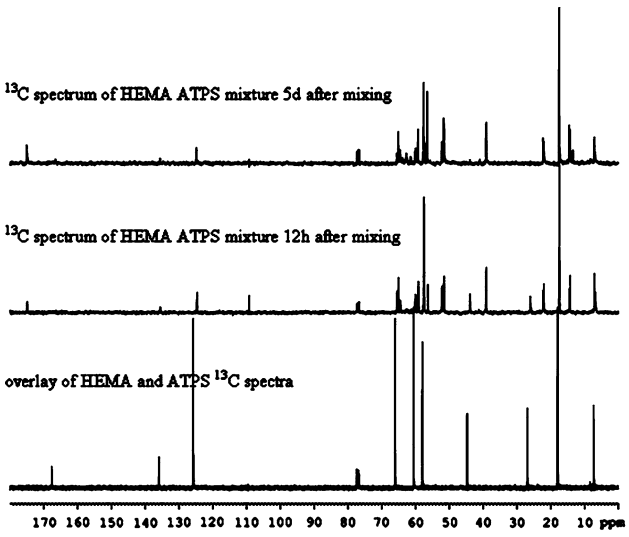

Fig. 1 ^{13}C NMR spectra of: overlay of HEMA and APTS; HEMA APTS mixture 12 h after mixing; HEMA APTS mixture 5 days after mixing

Table 2 ^{13}C NMR chemical shifts and functional group assignment of HEMA and ATPS in $CDCl_3$

HEMA		ATPS	
$-CH_3$	17.9	$-CH_3$	17.8
$-CH_2OH$	60.4	$-OCH_2-$	57.9
$-OCH_2-$	65.9	$SiCH_2-$	7.5
$=CH_2$	125.1	$-CH_2-$	26.4
$=C<$	135.9	H_2NCH_2-	44.3
C=O	167.8		

Indeed ESI(+)-MS of the samples (not reported) at 12 h and 5 days mixing time showed the presence of pseudo molecular peak at 352 m/z *product* while the ^{13}C spectra appeared markedly different from those of the starting material. In detail, the sp^2 region (double bonds) showed the clear loss of the signal at 125 ppm ($=CH_2$) and some variation in the chemical shifts of other signals; also the aliphatic region experienced a noteworthy signal proliferation symptomatic of new sigma bond formation. In particular the region 20–50 ppm (sp^3 C–N signals) showed the disappearance of the APTS signals (Fig. 1) together with parallel emerging of new ones.

Figure 2 shows FT-IR spectra obtained for HEMA and APTS mixture, just after mixing (Fig. 2a) and after 6 days at 40.0 °C (Fig. 2b).

In the high-frequency region ($\sim$3,400 cm^{-1}), HEMA had a wide and strong band centred at 3,429 cm^{-1} assigned to the OH stretching vibrations and due to the wide variety of hydrogen bonding between hydroxyl groups [31–33]. The APTS, HEMA mixture appears water free, in fact there is no evidence of bands at 2,130 and 1,650 cm^{-1} (H–O–H bending vibrations) and at about 700 cm^{-1} [34–36].

In the region 1,650–1,800 cm^{-1}, a very strong and sharp peak at 1,727 cm^{-1} corresponded to the stretching vibrations of carbonyl (C=O) groups [31–33]. The band located at 1,160 cm^{-1} was attributed to the stretching vibrations of C–O and proved the existence of ester groups in HEMA. The band between 2,700 and 3,100 cm^{-1} was associated with the symmetric and antisymmetric C–H stretching vibrations of CH_2 and CH_3 groups. Detailed information is listed in Table 3. These results are identical to those reported in the literature [37]. The peaks at around 1,090 cm^{-1} correspond to the Si–O stretching. The shoulder in the vicinity of the Si–O stretching mode (1,070–1,090 cm^{-1}) is due to the Si–O–C_2H_5 modes (1,100–1,165 cm^{-1}) [38]. Peaks at 960, 870 cm^{-1} correspond to Si–O–C_2H_5 modes and Si–C stretching. The band in the range 3,450–3,250 cm^{-1} can be attributed to N–H stretching, whereas those at 1,606 and 770 cm^{-1} correspond N–H in plane and out-of-plane deformation, respectively, in a primary amine [39].

Table 3 spectral band assignments for HEMA

Frequency (cm^{-1})	Possible assignments
3,439	ν (OH)
2,952	ν_{as} (CH_2, CH_3)
2,887	ν_s (CH_2, CH_3)
1,727	ν (C=O)
1,635	ν (C=C)
1,456–1,486	δ (CH_2)
1,365–1,390	CH_2 twist and rock
1,252–1,274	δ (OH)
1,160	ν (C–O)
1,077	ν (C–O–C)
850	δ (CH) rocking
750	ν (–C–O–)

As can be seen in Fig. 2b the band at 1,606 cm^{-1}, corresponding to N–H in plane deformation in a primary amine, disappears. Moreover, two peaks appear at 1,052 and 880 cm^{-1}, which can be attributed to C–O stretching and CH_2 rocking in ethanol. Furthermore the peak at 1,390 cm^{-1} shifts to lower wave numbers, 1,380 cm^{-1}, corresponding to CH_2 twisting and rocking in ethanol.

Figure 3 reports spectra of pHEMA (Fig. 3a) and pHEMA/SiO_2 gel hybrid (Fig. 3b).

pHEMA (Fig. 3a) spectrum exhibits typical absorption bands, including a strong peak at 1,715 cm^{-1}, assigned to C=O, and the broad band at 3,035–3,680 cm^{-1}, corresponding to O–H vibrations of side groups [31–33]. It is possible to notice the decrease in polymer content in hybrids. In fact, the peak at 1,715 cm^{-1} as well as other peaks assigned to polymer groups in the regions 2,880–2,950 and 1,380–1,480 cm^{-1} decrease in spectrum of

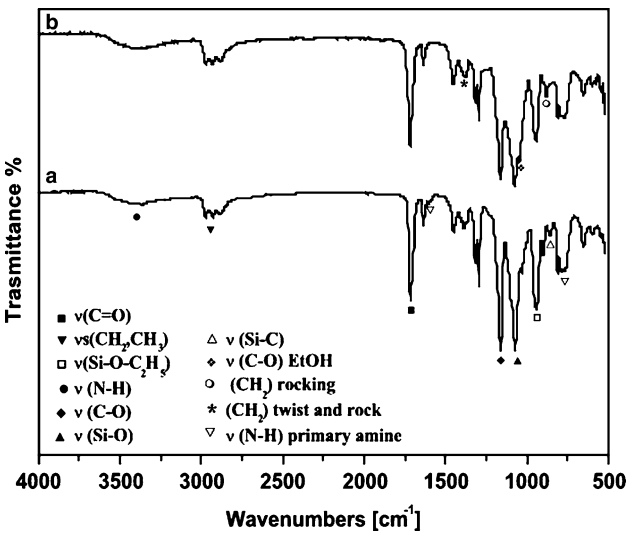

Fig. 2 FT-IR spectra obtained for HEMA and APTS mixture, just after mixing (**a**) and after 6 days at 40 °C (**b**)

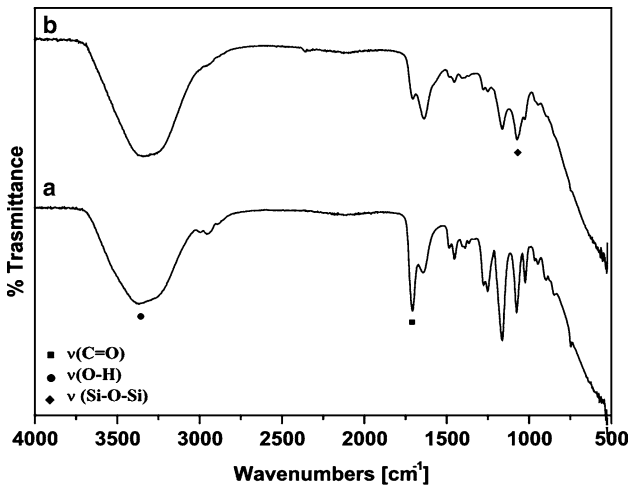

Fig. 3 FT-IR spectra of pHEMA (**a**) and pHEMA/SiO_2 hybrid (**b**)

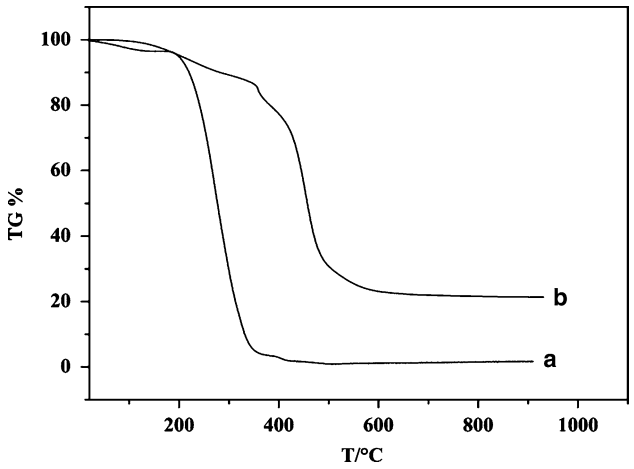

Fig. 4 TG curves of pHEMA (**a**) and pHEMA/SiO_2 hybrid (**b**)

hybrid and decrease in intensity comparatively to the peak at 1,630 cm^{-1}, which corresponds to free H_2O in porous structure. Figure 3b shows a marked increase of the band below 1,100 cm^{-1}. This is due to the overlapping of pHEMA groups with Si–O–Si stretching (1,100 cm^{-1}) [40, 41], thus confirming the presence of silica phase.

The hybrid composition was determined by thermal decomposition of the organic matrix in TG and Fig. 4 shows its thermogravimetric curve (Fig. 4b) compared to TG curve of pHEMA polymer (Fig. 4a). The degraded temperature (T_d) of the polymer phase was picked as the onset of the weight loss (starting from 280 °C in Fig. 4b). The T_d of pure pHEMA was 185 °C, whereas T_d of the hybrid was 280 °C. Therefore, pHEMA/SiO_2 gel nanocomposite exhibits better thermal stability than the as-prepared polymer [42].

The residual mass confirms a concentration of 30% w/w of silica gel to the mass of polymer. Figure 5 shows FT-IR spectrum of residual sample after thermal decomposition. The peak at 1,100 cm^{-1} can be attributed to Si–O–Si stretching vibration modes in SiO_4 units, that at 470 cm^{-1} is usually assigned to Si–O–Si bending, whereas the peak at 800 cm^{-1} is assigned to Si–O–Si bond vibration between two adjacent tetrahedra [40, 41], occurring in silica gel [43]. The shoulder at 950 cm^{-1} can be attributed to Si–O terminal non-bridging vibration [44, 45].

Figure 6 reports DSC curves of pHEMA (Fig. 6a) and pHEMA/silica hybrid (Fig. 6b). The slope changes in the temperature range 90–120 °C can be related to changes of specific heat in the glass transformation temperature (T_g). Taking T_g as the maximum of the derivative of DSC curve a value of 90 °C can be measured for glass transition temperature of pHEMA, whereas T_g of the nanocomposite is 112 °C. Therefore, the nanocomposite reveals an increase in the glass transition temperature.

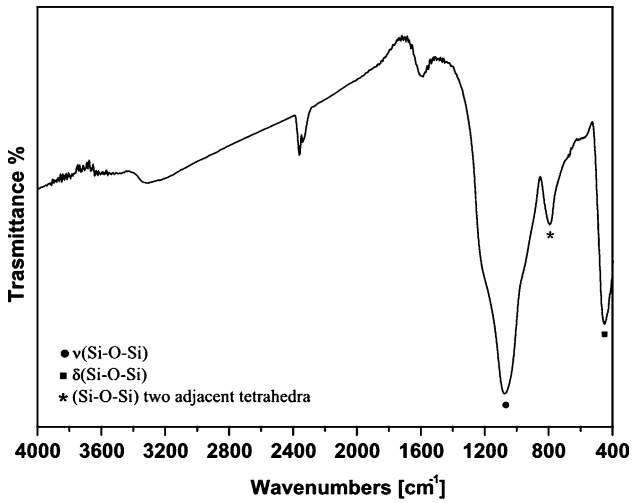

Fig. 5 FT-IR spectrum of residual sample after thermal decomposition in thermogravimetric up to 900 °C

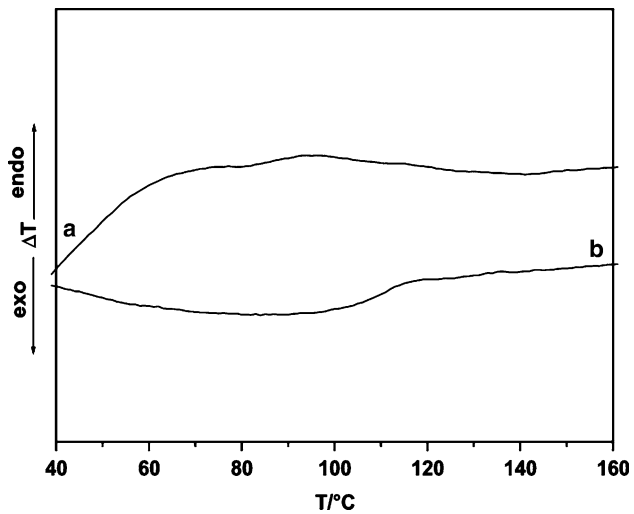

Fig. 6 DSC curves of pHEMA (**a**) and the hybrid (**b**)

A further characterization on the composite materials, in comparison to pHEMA, was obtained undertaking swelling experiments. The dry polymers were placed in distilled water and the water uptake was followed by gravimetric measurements at different times. Both materials reached saturation, showing similar equilibrium swelling: 67%. Small differences between swelling ratio values are within the experimental uncertainty (±2%).

Figure 7 shows TEM micrographs of the hybrid at low (Fig. 7a) and high magnification (Fig. 7b). Each reveals that, despite the optical transparency of the hybrid films, a microscopic heterogeneity exists. Both micrographs seems to indicate a two-phase morphology, but with a very fine texture, with domains of the darker inorganic phase of about 50 nm in size dispersed in the lighter organic phase. Moreover, the boundary between the inorganic and organic phases is indistinct even at the highest magnification (Fig. 7b), thus indicating a more intimate mixture of the two phases.

Figure 8 reports particles size distribution of the inorganic phase. The silica particles were distributed from 10 to 20 nm.

Figure 9 reports the FT-IR spectra for the hybrid material before (Fig. 9a) and after immersion in SBF for 14 days (Fig. 9b) and 21 days (Fig. 9c). As can be seen, after immersion in SBF, the bands assigned to the hybrid decrease in intensity, whereas three peaks appear at 561, 602 and 1037 cm^{-1}, which can be ascribed to P–O bending vibration and P–O stretching vibration, respectively [46].

Figure 10 reports SEM micrograph (Fig. 10a) and EDS spectrum (Fig. 10b) of as-prepared sample. Figure 11 shows SEM micrograph (Fig. 11a) and EDS spectrum (Fig. 11b) of a sample soaked for 14 days in SBF. For the same sample, Fig. 12 shows SEM micrograph at high

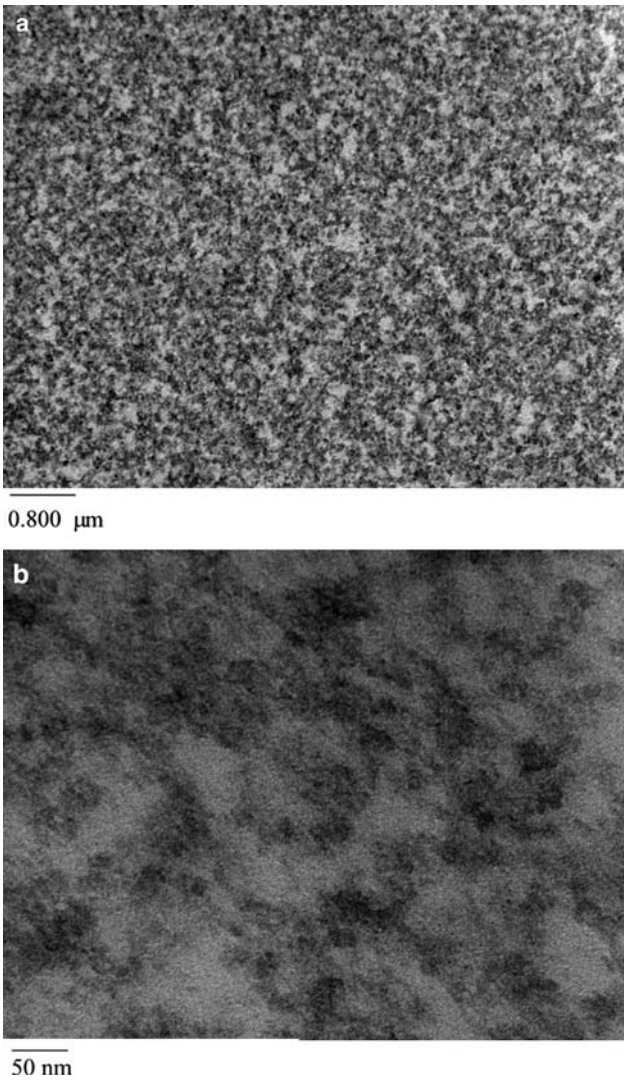

Fig. 7 TEM micrographs of the hybrid at low (**a**) and high magnification (**b**)

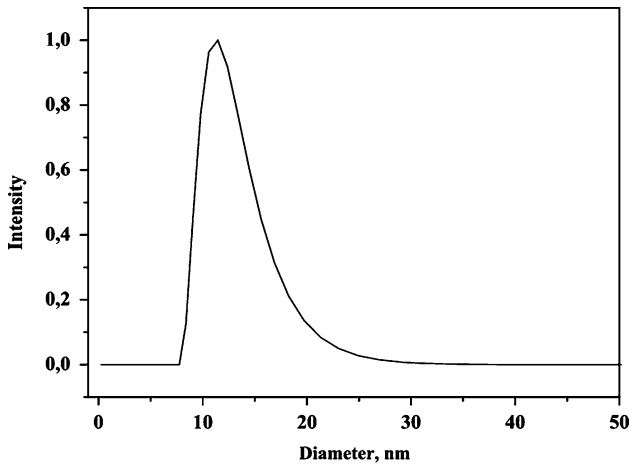

Fig. 8 Particles size distribution of the inorganic phase during the sol–gel process

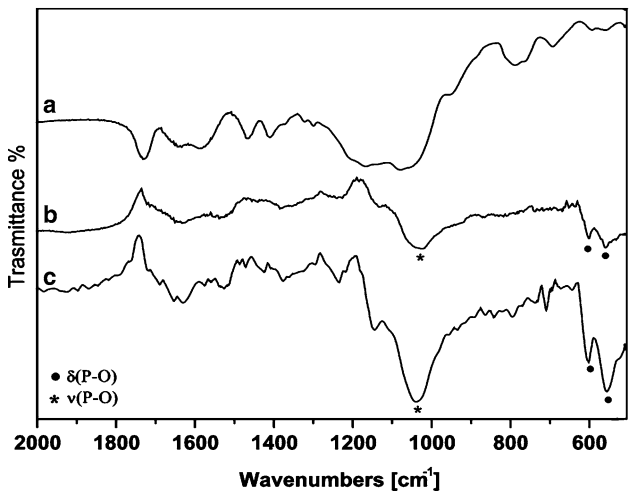

Fig. 9 FT-IR spectra for the hybrid material before (**a**) and after immersion in SBF for 14 days (**b**) and 21 days (**c**)

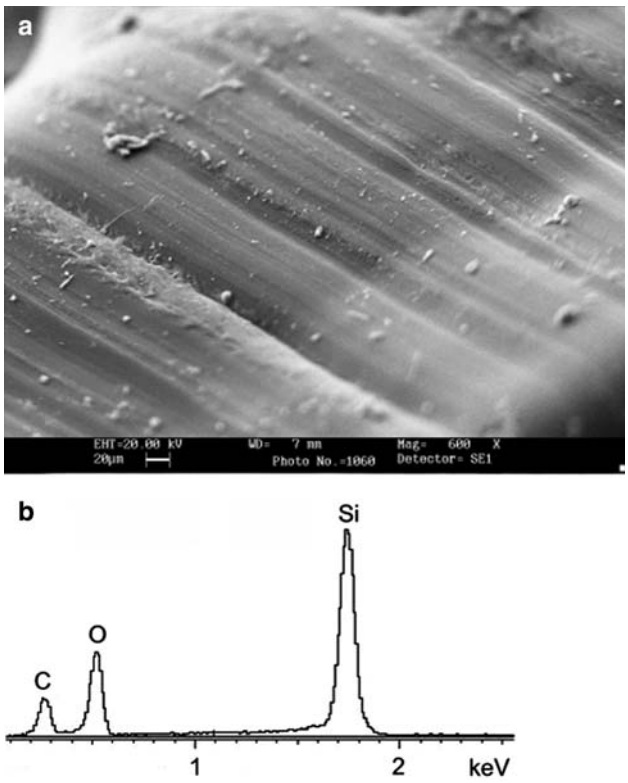

Fig. 10 SEM micrograph (**a**) and EDS spectrum (**b**) of as-prepared hybrid

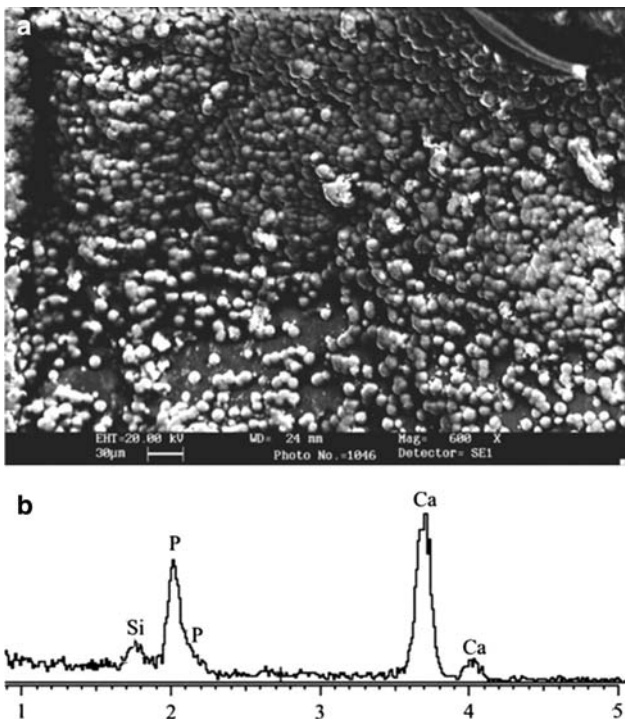

Fig. 11 SEM micrograph (**a**) and EDS spectrum (**b**) of the hybrid after 14 days' soaking in SBF

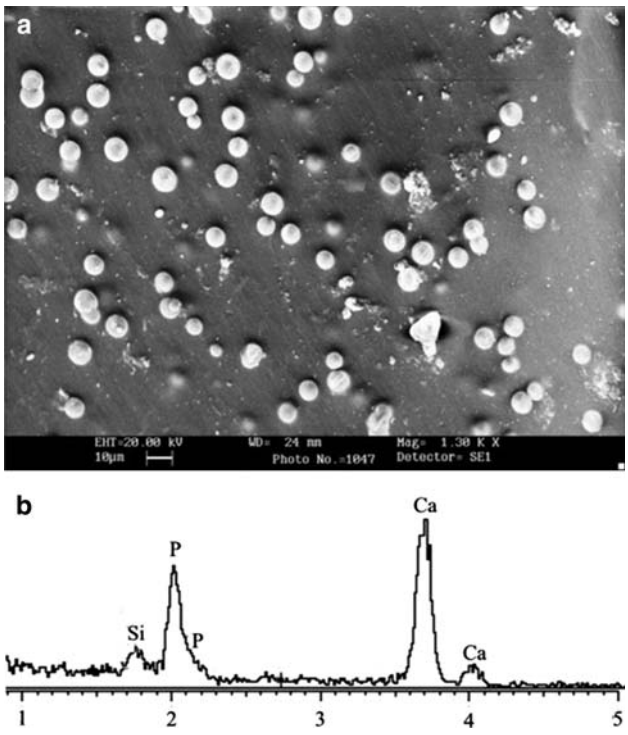

Fig. 12 High magnification SEM micrograph of a sample soaked for 14 days in SBF (**a**) and EDS spectrum obtained by spot analysis on a globular aggregate appearing beneath the surface (**b**)

magnification (Fig. 12a) and EDS spectrum obtained by spot analysis on a globular aggregate appearing beneath the surface (Fig. 12b). As can be seen the treatment in SBF has globular crystals formed on the polymer surface. EDS results (Fig. 11b) confirm they are apatite crystals, as it shows Ca and P peaks. Moreover, the presence of C and Si peaks in EDS spectrum proves that the apatite layer does not cover the whole surface. Furthermore, SEM micrograph and EDS spectrum at high magnification seem to indicate that globular crystals also forms beneath the surface. Figure 13 shows SEM micrograph (Fig. 13a) and EDS spectrum (Fig. 13b) of a sample soaked for 21 days in SBF. As can be seen the surface is uniformly covered by apatite globular crystals (Fig. 13a). This is confirmed by EDS spectrum (Fig. 13b) since Si peak is no longer present in the spectrum. Figure 14 show XRD pattern of a sample after 21 days' soaking in SBF. As can be seen, the pattern shows diffraction maxima at around 32° and 26° in two theta, characteristic of apatite-like phases.

4 Discussion

Even if the NMR pulse program used does not allow a direct comparison of signals of differently hybridized carbons, nonetheless an adequate quantitative evaluation of

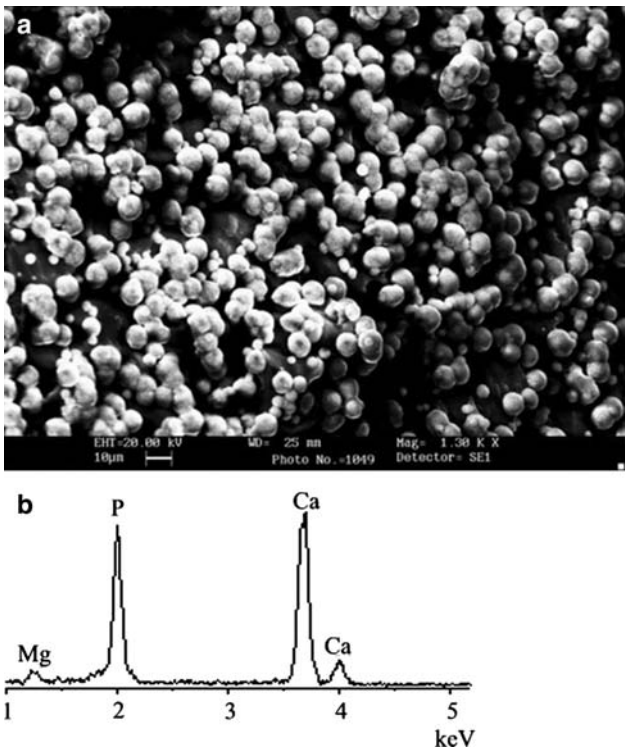

Fig. 13 SEM micrograph (**a**) and EDS spectrum (**b**) of a sample soaked for 21 days in SBF

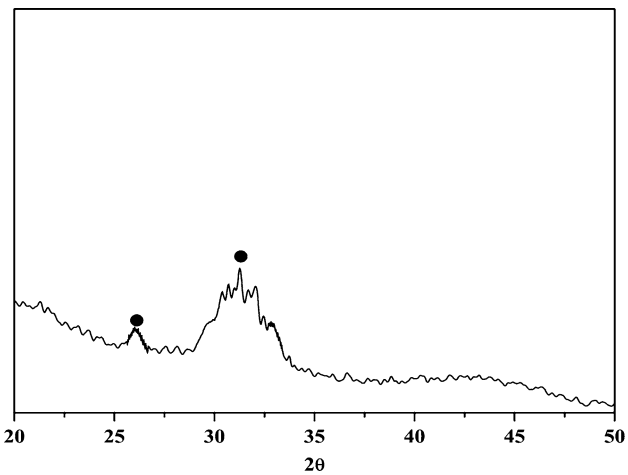

Fig. 14 XRD pattern of a sample soaked for 21 days in SBF: (•) apatite

reactant consumption may be obtained. In particular comparison of the two HEMA fast relaxing groups $=CH_2$ and $-CH_3$ (125.1 and 17.9 ppm, respectively) present a nearly 1:1 intensity ratio in the spectra of the sole reactant (Fig. 1), while after a 5 days reaction time this ratio decrease to less than 1:10 (Fig. 1). This variation is consistent with the structural modification at the olefin moiety leaving unchanged the methyl group as expected for the Michael addition. Moreover, in light of the similar relaxing time of carbons in these two groups, a residual of less than 10% of unreacted HEMA may be estimated.

Therefore, on the base ^{13}C NMR (Fig. 1) evidences and mass spectra data it was possible to ascertain the formation of coupling species between the nucleophilic amine and the Michael acceptor esther, according to the mechanism reported in Fig. 15.

This mechanism was proposed to account for the spectral data (as in Fig. 1), which are consistent with coupling reaction. Such a mechanism is reported in literature [28, 47], to occur on similar substrates and may well be called here for the first occurring processes after reagents mixing.

The organic–inorganic hybrid product of Michael addition is then present during radical polymerization of HEMA added in the second step of the synthesis.

Later processes may likely occur after and/or during the coupling as apparent from the ^{13}C signal proliferation with time. Such later processes may also involve other coupling/polymerizations as well as hydrolysis at different groups [48] this could also explain the some ethanol formation with time.

Moreover, the proposed reactions also account for FT-IR spectra of Fig. 2. In fact, the band 1,606 cm^{-1}, corresponding N–H in plane deformation in a primary amine, is no longer present in spectrum of Fig. 2b. Furthermore, absorption bands of ethanol appears in Fig. 2b.

When the organic polymer and the inorganic SiO_2 networks in hybrid materials produce minimal phase separation, the obtained hybrids can have good optical transparency and mechanical properties. Interactions between the polymer and the silica gel can inhibit macroscopic phase separation [49]. In particular by introducing a strong interactions between the silica network and the organic phase, the material can be made show little macroscopic phase separation [50]. Hence, the interaction

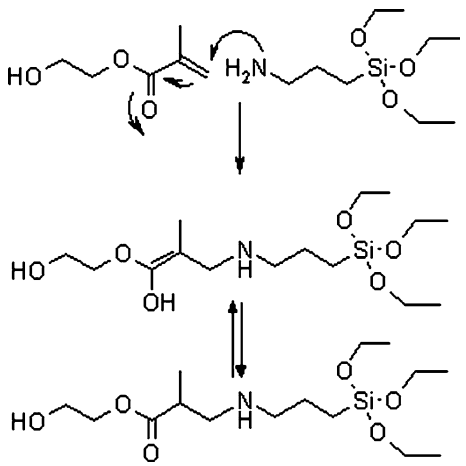

Fig. 15 HEMA APTS proposed reaction mechanism on the base of spectral data

between two phases plays a major role in controlling the properties of hybrid materials. The optical transparency can be used as an initial criterion for the formation of a homogeneous phase of both inorganic and organic constituents. When the macroscopic phase separation in the system occurs, the products look opaque because the large domain size of the inorganic oxide will cause light scattering in the system. The optical transparency of pHEMA/SiO_2 hybrid suggest that the organic–inorganic phase separation, if any, should be smaller than 400 nm in dimension. The absence of large-scale separations was further evidenced by SEM and TEM analysis. The latter (Fig. 7) proved a fine distribution of silica phase in the polymeric chains, with high uniformity. This can be explained considering the preparation of the hybrid via the inorganic–organic precursor route. In fact, as proposed by the mechanism reported in Fig. 15, APTS and HEMA react producing a hybrid monomer, which has a high affinity to the organic phase. Therefore, the strong interactions between the two phases inhibit the macroscopic phase separation.

The increase in the glass transition temperature (T_g) of the nanocomposite with respect to pHEMA (Fig. 6) can be explained by a good adhesion between the two phases and hence a reduced mobility of the pHEMA chains. The adhesion should be strong, because the silica particles are likely covered by hydroxyethyl-2-methylpropionate moieties on the surface and the same moieties are also present as repeat units in pHEMA. Besides this hydroxyl–hydroxyl (from hydroxyethyl in both phases) interactions can cause a mild physical cross-linking between the two phases. Finally, the hard, non-flexible silica domains present an obstacle to random chain segment movements of the pHEMA matrix. This effect (different from direct interaction of the two phases) is known in literature and as "topological constraint" and often can cause a T_g increase even if the phase's affinity to each other is poor [42].

pHEMA/SiO_2 swelling ratio is comparable to pHEMA (Fig. 7). In order to explain this result, we must consider that swelling ratio of hydrogels depends on their free volume, degree of the chain flexibility, and cross-link density and hydrophilicity [31]. The incorporation of rigid, non-swelling silica particles has swelling ratio decreased [27]. The presence of hydrated silica in a composite makes it more hydrophilic, thus having swelling ratio increased [14, 26]. The two effects are counterbalanced in the hybrid, thus making the swelling ratio similar to pHEMA.

The decrease of peaks characteristic of pHEMA/SiO_2 hybrid in FT-IR spectra of Fig. 9, suggests that immersion in SBF has the surface coated by a phosphate layer, as confirmed by the appearance of peaks assigned to PO_4 groups. This is confirmed by SEM/EDS results and XRD pattern (Fig. 14).

Li et al. have shown that even pure silica gels can induce nucleation and crystallisation of HA on their surfaces [51–53]. In fact, a widely accepted model suggest surface Si–OH groups act as nucleation sites for hydroxyapatite [52].

Furthermore, in previous works we proved that silica gel nanoparticles produced by sol–gel route using NH_3 as catalyst, were bioactive [14].

Therefore, we must conclude that silica gel phase keeps bioactive in the composite, thus having the material covered by a uniform apatite layer within 21 days.

Combining pHEMA and SiO_2 gel nanoparticles to make a nanocomposite is promising procedure to obtain a great variety of bioactive hydrogels without any surface modification as required in the past by the biomimetic method [25, 26].

Moreover, in situ prepared bioactive pHEMA-silica hybrid shows better bioactivity than pHEMA/SiO_2 nanocomposites, having the same silica content, but obtained by addition of silica nanoparticles to pHEMA solution [14]. Furthermore, it preserves optical transparency and swelling properties as pHEMA.

5 Conclusions

This article proposes a novel synthesis route to produce pHEMA/SiO_2 blend hybrids through an inorganic–organic hybrid monomer with pendant alkoxysilane groups, obtained from reaction of HEMA and APTS. The hybrid was obtained by basic catalysed sol–gel process of the alkoxysilane groups of the hybrid monomer and TEOS, followed by in situ polymerization of the hybrid monomer and HEMA.

The amounts of the inorganic precursor (TEOS), hybrid monomer and HEMA were chosen so as to have a final concentration of 30% w/w of silica gel to the mass of polymer.

The formation of coupling hybrid species between nucleophilic amine APTS and Michael acceptor HEMA was established on the base of ^{13}C NMR and mass spectra analysis.

Characterization of pHEMA-silica blend hybrid with a final concentration of 30% w/w of silica gel to the mass of polymer shows:

(1) No phase separation between the polymer and the silica gel, as strong interactions between the two phases inhibit the macroscopic phase separation.
(2) Improved thermal stability with respect to pHEMA.
(3) Higher glass transition temperature than pHEMA due to good adhesion between the two phases, physical cross-linking through hydroxyl–hydroxyl interactions and topological constraint.
(4) Similar swelling properties to pHEMA.

(5) Bioactive SiO_2 gel nanoparticles promote apatite formation on the surface of the hybrid hydrogel, when it is soaked in SBF. Therefore, the obtained bioactive hybrid can be used to make bioactive scaffold for bone engineering.

Acknowledgement The authors thank the Centro Interdipartimentale di Servizio per la Microscopia Elettronica (CISME) of Naples, for the transmission microscopy imaging.

References

1. Brinker CJ, Sherer W (1990) Sol–gel science: the physics and chemistry of sol–gel processing. Academic Press, San Diego
2. Wang B, Wilkes GL, Hedrick JC, Liptak BC, Mc Grath JE (1991) Macromolecules 24(11):3449–3450
3. Schmidt H, Krug H (1994) ACS Symp Ser 572:183
4. Huang HH, Orler B, Wilkes GL (1985) Polym Bull 14(6):557–564
5. Mark JE, Jiang CY, Tang MY (1984) Macromolecules 17(12): 2613–2616
6. Pope EJA, Asami M, Mackenzie JD (1989) J Mater Res 4(4):1018–1026
7. Wung CJ, Pang Y, Prasad PN, Karasz FE (1991) Polymer 32(4):605–608
8. Sung PH, Hsu TF (1998) Polymer 39(6–7):1453–1459
9. Reyes-Esqueda J, Darracq B, Garcia-Macedo J, Canva M, Blanchard-Desce M, Chaput F, Lahlil K, Boilot JP, Brun A, Levy Y (2001) Opt Commun 198(1–3):207–215
10. Wang B, Wilkes GL, Hedrick JC, Liptak SC, McGrath JE (1991) Macromolecules 24(11):3449–3450
11. Mackenzie JD, Huang Q, Iwamoto T (1996) J Sol–Gel Sci Technol 7(3):151–161
12. Mark JE (1996) Polym Eng Sci 36(24):2905–2920
13. Matejka L, Dukh O, Hlavata D, Brus J, Simonsick WJ Jr (2000) Polym Prepr 41(1):502
14. Costantini A, Luciani G, Annunziata G, Silvestri B, Branda F (2006) J Mater Sci Mater Med 17(4):319–325
15. Pereira MM, Jones JR, Orefice RL, Hench LL (2005) J Mater Sci Mater Med 16(11):1045–1050
16. Costa ROR, Pereira MM, Lameiras FS, Vasconcelos WL (2005) J Mater Sci Mater Med 16(10):927–932
17. Reetz MT (1997) Adv Mater 9(12):943–954
18. Ohtsuki C, Miyazaki T, Tanihara M (2002) Mater Sci Eng C C22(1):27–34
19. Wichterle O, Bartl P, Rosenberg M (1960) Nature 186(4723): 494–495
20. Peppas NA (ed) (1987) Hydrogels in medicine and pharmacy, vol I and II. CRC Press, FL
21. Netti PA, Shelton JC, Revell PA, Pirie C, Smith S, Ambrosio L, Nicolais L, Bonfield W (1993) Biomaterials 14(14):1098–1104
22. Montheard JP, Chatzopoulos M, Chappard D (1992) J Macromol Sci Rev Macromol Chem Phys C32(1):1–34
23. Hench LL (1991) J Am Ceram Soc 74(7):1487–1510
24. Kokubo T (1992) Proceedings of the XVI international congress on glass, Madrid, vol 1. S.E. de Ceramica y Vidrio, p 119
25. Branda F, Costantini A, Laudisio G, Buri A, Ambrosio L (1999) J Mater Sci 34(6):1319–1322
26. Branda F, Costantini A, Luciani G, Ambrosio L (2001) J Biomed Mater Res 57(1):79–83
27. Schiraldi C, D'Agostino A, Oliva A, Flamma F, De Rosa A, Apicella A, Aversa R, De Rosa M (2004) Biomaterials 25:3645–3653
28. Müh E, Marquardt J, Klee JE, Frey H, Muelhaupt R (2001) Macromolecules 34(17):5778–5785
29. Kokubo T, Hata K, Nakamura T, Yamamuro T (1991) In: Bonfield W, Hastings GW, Tanner KE (eds) Bioceramics, vol 4. Butterworth-Heinemann, Oxford
30. Tanahashi M, Hata K, Kokubo T, Minoda M, Miyamoto T, Nakamura T (1992) In: Yamamuro T, Kokubo T, Nakamura T (eds) Bioceramics, vol 5. Kobunshi-Kankokai, Kyoto
31. Bosch P, Del Monte F, Mateo JL, Levy D (1996) J Polym Sci A Polym Chem 34(16):3289–3296
32. Huang ZH, Qiu KY (1997) Polymer 38(3):521–526
33. Klee D, Hocker H (1999) Adv Polym Sci 149:1–57
34. Eisenberg D, Kauzmann W (1969) The structure and properties of water. Oxford University Press, London
35. Venyaminov SY, Prendergast FG (1997) Anal Biochem 248: 234–245
36. Ji XL, Jiang SC, Qiu XP, Dong DW, Yu DH, Jiang BZ (2003) J Appl Polym Sci 88(14):3168–3175
37. Perova TS, Vij JK, Xu H (1997) Coll Polym Sci 275(4):323–332
38. Mukherjee SP (1970) J Indian Chem Soc 47(11):1111–1116
39. Flett MSTC (1963) Characteristic frequencies of chemical groups in the infrared. Elsevier, Amsterdam
40. Ohtsuki C, Kokubo T, Yamamuro T (1992) J Non Cryst Sol 143(1):84–92
41. Kim CY, Clark AE, Hench LL (1989) J Non Cryst Sol 113(2–3): 195–202
42. Berriot J, Lequeux F, Montes H, Pernot H (2002) Polymer 43(23):6131–6138
43. Nyquist RA, Kagel RO (1991) Infrared spectra of inorganic compounds. Academic Press Inc., California
44. Bansal NP (1992) J Mater Sci 27(11):2922–2933
45. Huang Y, Jiang Z, Schwieger W (1999) Chem Mater 11(5):1210–1217
46. Hench LL, Andersson Ö (1993) In: Hench LL, Wilson J (eds) An introduction to bioceramics. World Scientific, Singapore
47. Colak S, Kusefoglu SH (2007) J Appl Polym Sci 104(4):2244–2253
48. Helminen A, Korhonen H, Seppala JV (2001) Polymer 42(8): 3345–3353
49. Landry CJT, Coltrain BK, Wesson JA, Zumbulyadis N, Lippert JL (1992) Polymer 33(7):1496–1506
50. Wei Y, Bakthavatchalam R, Yang D, Whitecar CK (1991) Polym Prepr 32(3):503–505
51. Li P, Ohtsuki C, Kokubo T, Nakanishi K, Soga N, Nakamura T, Yamamuro T (1992) J Am Ceram Soc 75(8):2094–2097
52. Pereira MM, Clark AE, Hench LL (1995) J Am Ceram Soc 78(9):2463–2468
53. Li P, Ohtsuki C, Kokubo T, Nakanishi K, Soga N, Nakamura T, Yamamuro T (1993) J Mater Sci Mater Med 4(2):127–131